IEEE Access
Multidisciplinary | Rapid Review | Open Access Journal

Received 24 December 2022, accepted 22 February 2023, date of publication 28 February 2023, date of current version 3 March 2023.

Digital Object Identifier 10.1109/ACCESS.2023.3250238

RESEARCH ARTICLE

Directional Pareto Front and Its Estimation to Encourage Multi-Objective Decision-Making

TOMOAKI TAKAGI, (Graduate Student Member, IEEE), KEIKI TAKADAMA, (Member, IEEE), AND HIROYUKI SATO, (Member, IEEE)

Graduate School of Informatics and Engineering, The University of Electro-Communications, Chofu, Tokyo 182-8585, Japan

Corresponding author: Tomoaki Takagi (tomtkg@uec.ac.jp)

ABSTRACT This work introduces the following concepts of directional and estimated directional Pareto front to encourage multi-objective decision making, especially when the Pareto front exists in limited regions in the objective space. The general output of multi-objective optimization is a set of non-dominated solutions to approximate the Pareto front. When the Pareto front exists in limited regions, few solutions are obtained and presented to the decision maker. The limited output representing the objective value trade-off is a barrier to multi-objective decision making. The directional Pareto front introduced in this study is a superset of the Pareto front and supplements the objective value trade-off between the Pareto fronts. The estimated directional Pareto front is a response surface that represents the directional Pareto front using a limited number of points, which are objective vectors of the obtained solutions. The experimental results show that the directional Pareto front and the estimated front provide an objective value trade-off even in areas where the Pareto front does not exist and enhances the explanation of the objective space of the target problem.

INDEX TERMS Multi-objective optimization, multi-objective decision-making, evolutionary algorithm, response surface methodology.

I. INTRODUCTION

Real-world optimization problems often involve multiple, conflicting objectives and become multi-objective optimization problems. The evolutionary algorithm is a powerful approach to tasks [1], [2]. Multi-objective optimization aims to acquire a solution set that approximates the Pareto front and optimal trade-off among multiple objectives. Pareto dominance is an essential criterion for comparing the solutions. Evolutionary multi-objective optimization generally outputs non-dominated solutions from the examined solutions during the search. After the optimization, we show the obtained non-dominated solution set to the decision maker. The decision maker then selects one of the non-dominated solutions while considering the objective value trade-off. This process is called multi-objective decision making [3]. Each multi-objective optimization problem has its own characteristics. Irregular Pareto front handling has received increasing attention in the research area of evolutionary multi-objective optimization [4], [5], [6], [7]. The irregular Pareto front has a region in which the Pareto front does not exist in the objective space. Pareto fronts commonly called degenerate, disconnected, and inverted ones are irregular. Research on irregular Pareto front handling aims to focus on the existing area of the Pareto front and obtain non-dominated solutions approximating the irregular Pareto front. However, acquiring only non-dominated solutions and showing them is not always the best method for multi-objective decision making, especially when the Pareto front exists in limited regions. In this case, the presentation of only non-dominated solutions may cause decision makers to have doubts and questions. Are there any other solutions to be an optimal trade-off? How do objective values change in non-existent areas of non-dominated solutions? These estimates would be increased by larger, non-existence regions of the Pareto front relative to the existence regions of the Pareto front in the objective space and cause a barrier in multi-objective decision-making. Explaining the non-existing areas of non-dominant solutions is a promising way to solve this issue.

The associate editor coordinating the review of this manuscript and approving it for publication was Danilo Pelusi.

In this study, we introduce the concept of the *directional Pareto front*, which is a superset of the Pareto front. The directional Pareto front involves an objective value trade-off even in regions where the Pareto front does not exist. The presentation of the directional Pareto front enhances the explanation of the objective value trade-off, particularly in the case where the Pareto front exists in limited regions. Clarifying the objective value changes in the non-existence area of the Pareto front would help in multi-objective decision-making. We also introduce the *estimated directional Pareto front*. The objective value trade-off is represented by points that are the objective vectors of the obtained solutions. The general method to increase the resolution of the objective value trade-off is to increase the number of points, solutions. However, this is often impossible, particularly for problems requiring computationally expensive objective functions. To address this issue, a unit hyperplane-based response surface method was proposed to estimate the Pareto front [8]. The estimated Pareto front continuously suggests the Pareto front using a response surface passing through the obtained objective vectors. We utilize this method to obtain the estimated directional Pareto front in this study. We select several evolutionary algorithms that acquire solutions to approximate the Pareto front and the directional Pareto front. We quantitatively and qualitatively assess the approximation qualities of the Pareto and directional Pareto fronts on several benchmark problems that have non-existence regions of the Pareto front in the objective space.

The contributions of this paper are summarized as follows:

1) The concept of directional Pareto front is proposed. The directional Pareto front is defined as objective vectors of non-dominated solutions on lines passing through the ideal point in the objective space. The directional Pareto front represents changes in the objective value even where the Pareto front does not exist. The directional Pareto front provides a guide for decision-making and understanding the target optimization problem, especially when the Pareto front exists in limited regions of the objective space.
2) It is shown that several evolutionary algorithms for acquiring directionally non-dominated solutions which approximate the directional Pareto front.
3) It is shown that the method and effect of directional Pareto front estimation, which estimates changes in objective values of the directional Pareto front between obtained objective vectors. The estimated Pareto front suggests changes in the objective value of the directional Pareto front even where objective vectors are not obtained.
4) A metric IGD' to evaluate the approximation quality of the directional Pareto front is proposed.

II. MULTI-OBJECTIVE OPTIMIZATION PROBLEM

A multi-objective optimization problem involves m objective functions $f_1, f_2, \ldots, f_m$ for a design variable vector $\boldsymbol{x} = (x_1, x_2, \ldots, x_d)$ in d-dimensional variable space $\mathcal{X}$ and is defined as

$$\text{Minimize } \boldsymbol{f}(\boldsymbol{x}) = (f_1(\boldsymbol{x}), f_2(\boldsymbol{x}), \ldots, f_m(\boldsymbol{x})). \tag{1}$$

The task is to acquire a solution set to approximate the optimal trade-off among the objective functions $f_1, f_2, \ldots, f_m$.

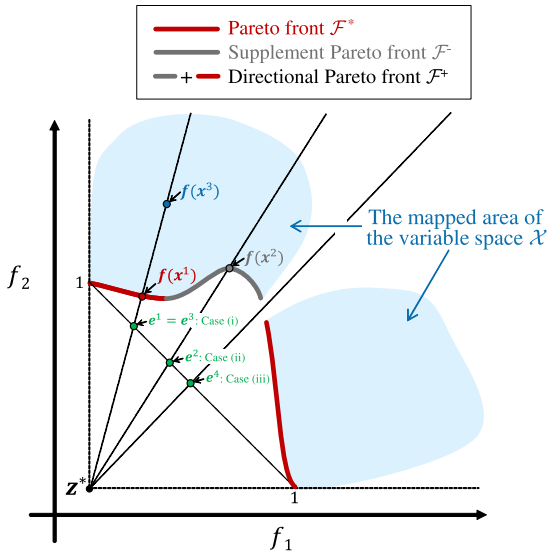

FIGURE 1. The Pareto front $\mathcal{F}^*$, the supplemental Pareto front $\mathcal{F}^-$, and the directional Pareto front $\mathcal{F}^+$.

III. PARETO FRONT AND ITS ESTIMATION

To represent the optimal trade-off among the objective functions, we describe the *Pareto front* and the *estimated Pareto front*.

A. DOMINANCE

The Pareto front requires *dominance*. For the two solutions, $\boldsymbol{x}$ and $\boldsymbol{y}$, $\boldsymbol{x}$ dominates $\boldsymbol{y}$ ($\boldsymbol{x} \preceq \boldsymbol{y}$) if and only if

$$\begin{aligned} &\forall i \in \{1, 2, \ldots, m\} : f_i(\boldsymbol{x}) \leq f_i(\boldsymbol{y} \wedge \\ &\exists j \in \{1, 2, \ldots, m\} : f_j(\boldsymbol{x}) < f_j(\boldsymbol{y}). \end{aligned} \tag{2}$$

B. PARETO FRONT

Among a set of solutions, those that are not dominated by any other solution are said to be *non-dominated solutions*. The non-dominated solutions in the variable space $\mathcal{X}$ are said to be *Pareto optimal solutions* $\mathcal{X}^* = \{\boldsymbol{x} \in \mathcal{X} \mid \nexists \boldsymbol{y} \in \mathcal{X} : \boldsymbol{y} \preceq \boldsymbol{x}\}$. The set of objective vectors of the Pareto optimal solutions $\mathcal{X}^*$ is called the *Pareto optimal front* $\mathcal{F}^* = \{\boldsymbol{f}(\boldsymbol{x}) \mid \boldsymbol{x} \in \mathcal{X}^*\}$. The Pareto optimal front is just called the *Pareto front* in this work.

Fig. 1 shows an example of $m = 2$ dimensional objective space. The red line represents the Pareto front, $\mathcal{F}^*$. The general output of multi-objective optimization is a set of non-dominated solutions to approximate the Pareto front $\mathcal{F}^*$.

C. ESTIMATED PARETO FRONT

1) OVERVIEW

A non-dominated solution set represents the objective trade-off as a point set in the objective space. The general method

to increase the resolution of the objective trade-off is to increase the number of points, examined solutions. However, we often face limitations in increasing the number of solution evaluations; for example, the execution of objective functions requires computationally expensive calculations. For this situation, Pareto front estimation has been studied so far. It estimates the Pareto front in the objective space where the objective vectors of examined solutions do not exist and/or the Pareto optimal solutions in the variable space where the examined solutions do not exist.

2) RELATED WORKS

Polynomial function fitting has been employed for the Pareto front estimation. A generalized polynomial function is given by $\alpha_1 f_1^{\beta_1} + \alpha_2 f_2^{\beta_2} + \ldots + \alpha_m f_m^{\beta_m} = 1$. A single scalar $\beta_1 = \beta_2 = \ldots = \beta_m$ was adjusted in [9] and [10] with fixed $\boldsymbol{\alpha} = (1, 1, \ldots, 1)$. A single vector $\boldsymbol{\alpha} = (\alpha_1, \alpha_2, \ldots, \alpha_m)$ was adjusted in [11] with fixed $\boldsymbol{\beta} = (1, 1, \ldots, 1)$. Both vectors $\boldsymbol{\alpha}$ and $\boldsymbol{\beta}$ were adjusted in [12]. For complicated Pareto fronts, the combination of different polynomial functions was proposed [13]. Note that the above polynomial function fitting approach estimates the Pareto front during multi-objective optimization online and utilizes the estimated Pareto front as search guidance.

Mainly for the resolution enhancement of the Pareto front as the post process of multi-objective optimization, PAINT (PAreto INTerpolation) was proposed [14]. PAINT first generates a set of simplexes constructed by combinations of given objective vectors as vertices. PAINT then eliminates certain simplexes by using several dominance-related rules and outputs the remained simplexes as a result. PLI (Pareto Liner Interpolation), an extension of PAINT, employs a set of uniformly distributed reference vectors and provides interpolation points as intersections of simplexes and reference vectors [15], [16]. Also, as the generalized Bézier curve fitting, the Bézier simplex fitting was proposed for the Pareto front estimation [17].

The response surface approach [18] has been employed for estimating the Pareto optimal solutions and the Pareto front. The radial basis function neural network (RBFNN) [19], [20] was employed in [21] and [22], and its model was trained by objective vectors assuming a subset of the Pareto front and their variable vectors assuming a subset of the Pareto optimal solutions. The output is a set of estimated Pareto optimal solutions in the variable space, and the estimated Pareto front is obtained by executing the objective functions to the estimated Pareto optimal solutions. The Kriging [23], [24] was employed in [8], and its model was trained by known objective vectors assuming a subset of the Pareto front. The output is an estimated Pareto front in the objective space without considering the variable space. A characteristic of the Kriging-based Pareto front estimation expresses both the estimated objective vectors and their confidence levels.

In this paper, we pick the Kriging-based Pareto front estimation proposed in [8] for the following reasons: (i) we focus on a post-process of multi-objective optimization to improve the resolution of the Pareto front not on the multi-objective optimization, (ii) we focus only on the Pareto front in the objective space and not on the Pareto optimal solutions in the variable space, (iii) the Kriging-based Pareto front estimation can obtain the estimated Pareto front without additional executions of the objective functions after the estimation model is trained, and (iv) the Kriging-based Pareto front estimation can provide not only estimated objective vectors but also their confidence levels.

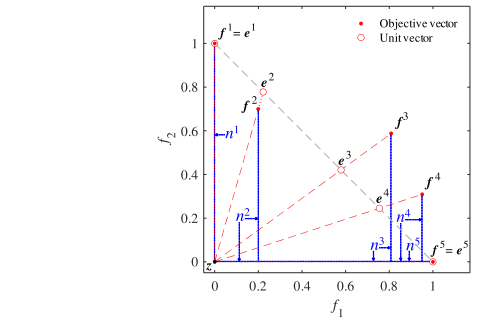

(a) Inputs $e^1, e^2, \ldots, e^5$ and outputs $n^1, n^2, \ldots, n^5$

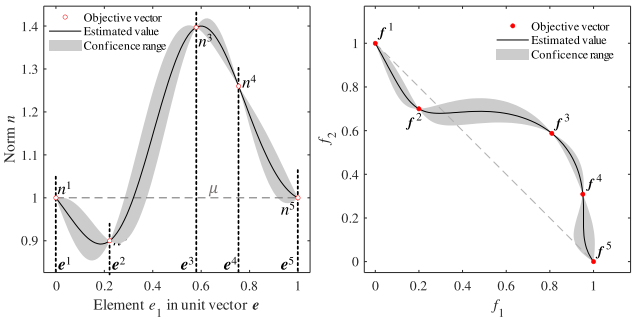

(b) Estimated norm (c) Estimated objective value

FIGURE 2. Objective value estimation using response surface based on the unit hyperplane [8].

3) KRIGING-BASED PARETO FRONT ESTIMATION

The Kriging-based Pareto front estimation [8] generates an estimated Pareto front as a Kriging-based response surface based on the unit hyperplane in the objective space. The generated response surface passes through the points of solutions obtained in the objective space.

This method requires an objective vector set that corresponds to a solution set obtained through optimization. First, we transform each objective vector $\boldsymbol{f}$ into its L^1-norm $n(\boldsymbol{f}) = \sum_{i=1}^{m} f_i$ and its L^1-unit vector $\boldsymbol{e}(\boldsymbol{f}) = \boldsymbol{f}/n(\boldsymbol{f})$. We then generate a Kriging-based estimation model [24] based on L^1 unit vector set as the input and L^1 norm set as the output. The generated Kriging-based estimation model outputs an estimated L^1 norm $\hat{n}$ for any L^1 unit vector, $\boldsymbol{e}$. The estimated L^1-norm $\hat{n}$ can be converted into the estimated objective vector $\hat{\boldsymbol{f}}$ $(= \hat{n} \cdot \boldsymbol{e})$. In other words, the generated Kriging-based

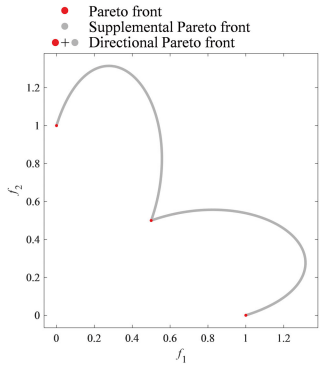

FIGURE 3. DTLZ1S2 problem.

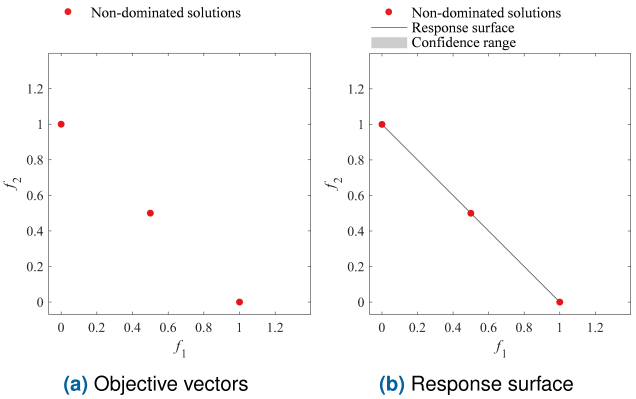

FIGURE 4. Pareto front approximation of DTLZ1S2.

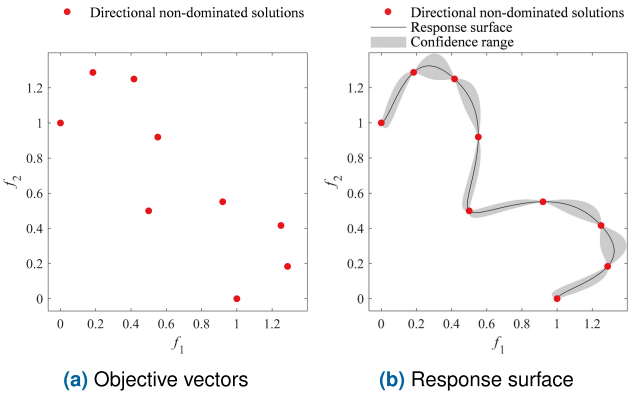

FIGURE 5. Directional Pareto front approximation of DTLZ1S2.

estimation model provides an estimated objective vector $\hat{\boldsymbol{f}}$ for a given L^1 unit vector $\boldsymbol{e}$, which indicates the direction in the objective space. We input a large uniformly distributed L^1 unit vector set $\mathcal{E}$ to the generated Kriging-based estimation model. The output is the estimated Pareto front, $\hat{\mathcal{F}}^* = \{\hat{n} \cdot \boldsymbol{e} \mid \boldsymbol{e} \in \mathcal{E}\}$. Because the estimation model is generated by the Kriging method, the confidence level of the estimation can also be represented.

Fig. 2 shows an example with $m = 2$ objectives. We have five examined solutions, and their objective vectors $\boldsymbol{f}^1, \boldsymbol{f}^2, \ldots, \boldsymbol{f}^5$ are shown as filled red circles. First, in **Fig. 2 (a)**, for each objective vector, we calculate its L^1 norm n depicted as a blue line, and unit vector $\boldsymbol{e}$ shown as an open red circle. Then, we generate Kriging-based estimation model based on the obtained unit vectors $\boldsymbol{e}^1, \boldsymbol{e}^2, \ldots, \boldsymbol{e}^5$ as inputs and their norms $n^1, n^2, \ldots, n^5$ as outputs. **Fig. 2 (b)** shows estimated norms $\hat{n}$ obtained by the generated Kriging model. The horizontal axis is set as an element e_1 of the unit vector $\boldsymbol{e} = (e_1, e_2)$. The five open circles correspond to five known objective vectors. The black line is the estimated $\hat{n}$ output from the generated Kriging model by inputting a large uniformly distributed unit vector set $\mathcal{E}$. The gray area represents the confidence range, which was also obtained from the Kriging model. **Fig. 2 (b)** can be projected to the objective space shown as **Fig. 2 (c)** by using $\hat{n} \cdot \boldsymbol{e} = \hat{\boldsymbol{f}}$, and the black line in **Fig. 2 (c)** becomes the estimated Pareto front $\hat{\mathcal{F}}^*$ in this case. Thus, a limited number of objective vectors $\boldsymbol{f}^1, \boldsymbol{f}^2, \ldots, \boldsymbol{f}^5$ can be complemented by the estimated Pareto front $\hat{\mathcal{F}}^*$.

IV. ISSUE FOCUS: INSUFFICIENT REPRESENTATION OF OBJECTIVE VALUE CHANGE

A. SAMPLE PROBLEM

We use DTLZ1Sρ problem, which is defined as

$$f_j(\boldsymbol{x}) = f_j^{\mathrm{DTLZ1}}(\boldsymbol{x}) \cdot 2\left(1 + \frac{\rho \cdot |\sin(2\pi x_1)|}{3}\right) \times (j = 1, 2, \ldots, m), \quad (3)$$

where f_j^{DTLZ1} is the jth objective function of the DTLZ1 problem [25], which is a frequently used benchmark problem.

Fig. 3 shows an $m = 2$ dimensional objective space of the DTLZ1S2 problem, which is the DTLZ1Sρ with $\rho = 2$. DTLZ1S2 has only three Pareto optimal solutions, and the Pareto front is $\mathcal{F}^* = \{(1.0, 0.0), (0.5, 0.5), (0.0, 1.0)\}$. **Fig. 3** shows the Pareto front $\mathcal{F}^*$ with the red points. The gray-dominated points indicate the objective value change between the separated Pareto front parts.

B. VISUAL EXAMPLE

Fig. 4 (a) shows a non-dominated solution set approximating the Pareto front $\mathcal{F}^*$ for the DTLZ1S2 problem. **Fig. 4 (b)** shows the estimated Pareto front $\hat{\mathcal{F}}^*$ generated by the non-dominated solution set shown in **Fig. 4 (a)**.

From **Fig. 4 (a)**, the decision maker sees three non-dominated solutions. The decision-maker cannot see the objective value change between two neighboring non-dominated solutions. The decision-maker cannot even see whether there are solutions between two neighboring non-dominated solutions.

Fig. 4 (b) shows a black line passing through three non-dominated solutions. The black line represents the response surface, which is the estimated Pareto front $\hat{\mathcal{F}}^*$. Because the estimated Pareto front $\hat{\mathcal{F}}^*$ is constructed only from the three non-dominated points, it differs from the actual objective value change shown by the gray points in **Fig. 3**. The decision

maker will misunderstand the objective value change from the estimated Pareto front $\hat{\mathcal{F}}^*$ generated by the solutions distributed in limited areas in the objective space.

When the Pareto front $\mathcal{F}^*$ exists in limited regions, the presentation of only non-dominated solutions may cause the decision maker to have doubts and questions. Are there no other non-dominated solutions? How do objective values change in non-existent areas of non-dominated solutions? These doubts and questions may hinder multi-objective decision-making. Explaining the non-existent areas of non-dominated solutions is a promising way to solve this issue. However, when the obtained solutions are distributed in limited areas, we cannot expect the accuracy of the estimated Pareto front $\hat{\mathcal{F}}^*$ constructed using the obtained non-dominated solutions. If we could represent the objective value change even in non-existence areas of the non-dominated solutions, it would enhance the explanation of the objective space to the decision maker and encourage multi-objective decision-making.

V. DIRECTIONAL PARETO FRONT AND ITS ESTIMATION

To represent the objective value trade-off, even in areas where the Pareto front does not exist, we introduce the concepts of *directional Pareto front* and *estimated directional Pareto front*.

A. DIRECTIONAL DOMINANCE

A directional Pareto front requires the concept of *directional dominance*. For two solutions $\boldsymbol{x}$ and $\boldsymbol{y}$, in this study, we say that $\boldsymbol{x}$ directionally dominates $\boldsymbol{y}$ ($\boldsymbol{x} \preceq^+ \boldsymbol{y}$) if and only if

$$\boldsymbol{e}(\boldsymbol{f}'(\boldsymbol{x})) = \boldsymbol{e}(\boldsymbol{f}'(\boldsymbol{y})) \wedge \boldsymbol{x} \preceq \boldsymbol{y}, \tag{4}$$

where $\boldsymbol{e}(\boldsymbol{f}')$ is the L^1 unit vector of normalized objective vector $\boldsymbol{f}'$ described in Section III-C, $\boldsymbol{f}' = \frac{\boldsymbol{f}-\boldsymbol{z}^*}{\boldsymbol{n}^*-\boldsymbol{z}^*}$, $\boldsymbol{z}^* = (z_1^*, z_2^*, \ldots, z_m^*)$ is the ideal point, its elements are $z_i^* = \min_{\boldsymbol{x}\in\mathcal{X}} f_i(\boldsymbol{x})$ $(i = 1, 2, \ldots, m)$, $\boldsymbol{n}^* = (n_1^*, n_2^*, \ldots, n_m^*)$ is the nadir point, its elements are $n_i^* = \max_{\boldsymbol{x}\in\mathcal{X}'} f_i(\boldsymbol{x})$ $(i = 1, 2, \ldots, m)$. The first condition is the equality of two L^1 unit vectors in the objective space. The second condition is the conventional dominance criterion described in Section III-A. Thus, the directional dominance criterion compares two objective vectors sharing the same unit vector by the conventional dominance.

We explain the directional dominance relation using the visual example shown in **Fig. 1**. **Fig. 1** has three objective vectors $\boldsymbol{f}(\boldsymbol{x}^1)$, $\boldsymbol{f}(\boldsymbol{x}^2)$, and $\boldsymbol{f}(\boldsymbol{x}^3)$ respectively depicted by red, gray, and blue filled circles. Their unit vectors $\boldsymbol{e}^1$, $\boldsymbol{e}^2$, and $\boldsymbol{e}^3$ are respectively depicted as green circles. First, we compare $\boldsymbol{x}^1$ and $\boldsymbol{x}^2$. Their unit vectors $\boldsymbol{e}^1$ and $\boldsymbol{e}^2$ are different, that is, $\boldsymbol{e}^1 \neq \boldsymbol{e}^2$. Since the first condition of **Eq. (4)** is not satisfied, we say $\boldsymbol{x}^1$ and $\boldsymbol{x}^2$ are directionally non-dominated by each other. Next, we compare $\boldsymbol{x}^1$ and $\boldsymbol{x}^3$. Their unit vectors $\boldsymbol{e}^1$ and $\boldsymbol{e}^3$ are the same, that is, $\boldsymbol{e}^1 = \boldsymbol{e}^3$. Since the first condition of **Eq. (4)** is satisfied, we then compare $\boldsymbol{x}^1$ and $\boldsymbol{x}^3$ using the conventional dominance for the second condition of **Eq. (4)**. We see $\boldsymbol{x}^1$ dominates $\boldsymbol{x}^3$, that is, $\boldsymbol{x}^1 \preceq \boldsymbol{x}^3$. Since both the first and second conditions of **Eq. (4)** are satisfied, we say $\boldsymbol{x}^1$ directionally dominates $\boldsymbol{x}^3$, that is, $\boldsymbol{x}^1 \preceq^+ \boldsymbol{x}^3$.

B. DIRECTIONAL PARETO FRONT

In this study, the directionally non-dominated solutions in the variable space $\mathcal{X}$ are said to be *directional Pareto optimal solutions* $\mathcal{X}^+ = \{\boldsymbol{x} \in \mathcal{X} \mid \nexists \boldsymbol{y} \in \mathcal{X} : \boldsymbol{y} \preceq^+ \boldsymbol{x}\}$, and the set of objective vectors of the directional Pareto optimal solutions $\mathcal{X}^*$ is said to be the *directional Pareto front* $\mathcal{F}^+ = \{\boldsymbol{f}(\boldsymbol{x}) \mid \boldsymbol{x} \in \mathcal{X}^+\}$. Each objective vector $\boldsymbol{f}(\boldsymbol{x}) \in \mathcal{F}^+$ is closest to the ideal point $\boldsymbol{z}^*$ on the line passing through $\boldsymbol{f}(\boldsymbol{x})$ and the ideal point $\boldsymbol{z}^*$ in the objective space. In this study, the difference between the directional Pareto front $\mathcal{F}^+$ and Pareto front $\mathcal{F}^*$ is said to be the *suppremental Pareto front* $\mathcal{F}^- (= \mathcal{F}^+ \backslash \mathcal{F}^*)$.

The visual example of **Fig. 1** shows the Pareto front $\mathcal{F}^*$ with the red lines, the supplemental Pareto front $\mathcal{F}^-$ with the gray line, and the directional Pareto front $\mathcal{F}^+$ with the combined red and gray lines. We assume that $\boldsymbol{x}^1$ is a Pareto optimal solution and a directional Pareto optimal solution, i.e. $\boldsymbol{x}^1 \in \mathcal{X}^*$ and $\boldsymbol{x}^1 \in \mathcal{X}^+$. Consequently, objective vector $\boldsymbol{f}(\boldsymbol{x}^1)$ is a member of the Pareto front $\mathcal{F}^*$ and also the directional Pareto front $\mathcal{F}^+$, i.e. $\boldsymbol{f}(\boldsymbol{x}^1) \in \mathcal{F}^*$ and $\boldsymbol{f}(\boldsymbol{x}^1) \in \mathcal{F}^+$. $\boldsymbol{x}^2$ is dominated by $\boldsymbol{x}^1$ and not a Pareto optimal but we assume that $\boldsymbol{x}^2$ is a directional Pareto optimal solution, i.e. $\boldsymbol{x}^2 \in \mathcal{X}^+$. Consequently, objective vector $\boldsymbol{f}(\boldsymbol{x}^2)$ is a member of the directional Pareto front $\mathcal{F}^+$, i.e. $\boldsymbol{f}(\boldsymbol{x}^2) \in \mathcal{F}^+$. $\boldsymbol{x}^3$ is dominated by solutions including $\boldsymbol{x}^1$. Also, $\boldsymbol{x}^3$ is directionally dominated by solutions including $\boldsymbol{x}^1$ on the radial line passing through the ideal point and the objective vector $\boldsymbol{f}(\boldsymbol{x}^3)$ in the objective space. From **Fig. 1**, we see the red Pareto front includes $\boldsymbol{f}(\boldsymbol{x}^1)$ but not $\boldsymbol{f}(\boldsymbol{x}^2)$. We see the combined red and gray directional Pareto front includes both $\boldsymbol{f}(\boldsymbol{x}^1)$ and $\boldsymbol{f}(\boldsymbol{x}^2)$. Thus, the directional Pareto front involves dominated objective vectors such as $\boldsymbol{f}(\boldsymbol{x}^2)$ if they are non-dominated on their radial lines. $\boldsymbol{x}^2$ is not preferred in general multi-objective optimization since solutions including $\boldsymbol{x}^1$ dominate $\boldsymbol{x}^2$. However, directionally non-dominated solutions such as $\boldsymbol{x}^2$ represent the trade-off among objective values even though they are dominated in the viewpoint of the conventional dominance, and they would help to further explain the objective space and encourage multi-objective decision-making.

Here, note that each unit vector $\boldsymbol{e}$ in **Fig. 1** can be classified into one of the following three cases.

Case (i): If the non-dominated solution exists on the unit vector $\boldsymbol{e}$, it passes through the Pareto front in red.

Case (ii): If the non-dominated solution does not exist but at least one dominated solution exists on the unit vector $\boldsymbol{e}$, it passes through the supplemental Pareto front in gray.

Case (iii): If any solutions do not exist on the unit vector $\boldsymbol{e}$, it does not pass both the Pareto front in red and the supplemental Pareto front in gray.

In **Fig. 1**, $\boldsymbol{e}^1$ and $\boldsymbol{e}^3$ are the case (i), $\boldsymbol{e}^2$ is the case (ii), and $\boldsymbol{e}^4$ is the case (iii). **Fig. 1** involves the mapped areas of the variable space $\mathcal{X}$ with light blue. The case (iii) arises

due to the absence of these areas in the objective space. The cases (ii) and (iii) represent the non-existent area of the Pareto front.

C. ESTIMATED DIRECTIONAL PARETO FRONT

To obtain the *estimated directional Pareto front*, we utilize the unit hyperplane-based response surface method [8] mentioned in Section III-C. In Section III-C, we obtained the estimated Pareto front $\hat{\mathcal{F}}^*$ by inputting non-dominated solutions. On the other hand, we obtain the estimated directional Pareto front $\mathcal{F}^+$ by inputting the directionally non-dominated solutions. In other words, the input data are different from the conventional Pareto front estimation [8] described in Section III-C. After the estimation model is generated, we input a large, uniformly distributed L^1 unit vector set $\mathcal{E}$ into the estimation model and obtain an estimated objective vector set, which is the estimated directional Pareto front $\hat{\mathcal{F}}^+ = \{\hat{n} \cdot \boldsymbol{e} \mid \boldsymbol{e} \in \mathcal{E}\}$. Similar to the estimated Pareto front $\hat{\mathcal{F}}^*$, the confidence level of the estimated directional Pareto front $\hat{\mathcal{F}}^+$ can be represented as well.

D. VISUAL EXAMPLE

Fig. 5 (a) shows a directionally non-dominated solution set approximating the directional Pareto front $\mathcal{F}^+$ of the DTLZ1S2 problem. **Fig. 5 (b)** shows the estimated directional Pareto front $\hat{\mathcal{F}}^+$ obtained by the same directionally non-dominated solution set.

The directionally non-dominated solutions shown in **Fig. 5 (a)** represent not only the Pareto front $\mathcal{F}^*$ but also the supplemental Pareto front $\mathcal{F}^-$. The decision maker can see the objective value change between the separated Pareto fronts $\mathcal{F}^*$. In **Fig. 5 (b)**, the black line passing through the directionally non-dominated solutions is the response surface, which is the estimated directional Pareto front $\hat{\mathcal{F}}^+$. It continuously represents the objective value change between separated Pareto fronts $\mathcal{F}$. The gray areas represent the confidence levels of the estimated directional Pareto front.

VI. MULTI-OBJECTIVE EVOLUTIONARY ALGORITHMS

A. OVERVIEW

In each of multi-objective evolutionary algorithms, its solution comparison criterion impacts the characteristics of the obtained solution set.

The majority of algorithms employ the dominance described in Section III-A. Several criteria extending dominance have been studied. The ϵ-dominance [26], the expanded dominance [27], and the cone ϵ-dominance [28] expand the dominance area and encourage to dominate other solutions. They make fine-grained solution rankings and strengthen the selection pressure for the search. These methods work to obtain solutions to approximate the Pareto front but not to approximate the directional Pareto front.

θ-dominance [29] and SDR (strengthened dominance relation) [30], [31] have a common concept, which suppresses the influence range of dominance in the objective space. These criteria make fine-grained solution rankings inside the influence range. These criteria can be viewed as relaxed versions of the directional dominance to encourage solution comparisons. These criteria work to acquire solutions to approximate not only the Pareto front but also the directional Pareto front.

Several criteria using sacralized objective values have also been studied. The Tchebycheff distance [32], [33] determines the superiority of solutions for a given weight vector and is compliant with the dominance. The Tchebycheff distance works to acquire solutions to approximate the Pareto front.

PBI (penalty-based boundary intersection) [34] and APD (angle-penalized distance) [35] determines the superiority of solutions for a given weight vector based on the relations between the weight vector and the objective vectors. For the directional difference between a weight vector and an objective vector, PBI uses the perpendicular distance between them, and APD uses the angles between them. These criteria can be viewed as relaxed versions of the directional dominance to encourage solution comparisons. These criteria work to acquire solutions to approximate not only the Pareto front but also the directional Pareto front.

As algorithms employing the above criteria, in this study, we selected MOEA/D [34], NSGA-III [36], NSGA-II/SDR [30], θ-DEA [29], and RVEA [35] based algorithms.

B. MOEA/D-rTCH AND MOEA/D-PBI

MOEA/D [34] optimizes m objective functions using a set of weight vectors to decompose the objective space. MOEA/D prepares a set of uniformly distributed weight vectors, $\mathcal{L} = \{\boldsymbol{\lambda}^1, \boldsymbol{\lambda}^2, \ldots, \boldsymbol{\lambda}^N\}$. Each weight vector $\boldsymbol{\lambda}^j = (\lambda_1^j, \lambda_2^j, \ldots, \lambda_m^j)$ denotes a point on the unit hyper plane. For each weight vector $\boldsymbol{\lambda}^j$, we assign one solution $\boldsymbol{x}^j$ and construct the population $\mathcal{P} = \{\boldsymbol{x}^1, \boldsymbol{x}^2, \ldots, \boldsymbol{x}^N\}$. Newly generated solutions are compared based on their scalarizing function values using weight vectors. In this study, we select MOEA/D-rTCH using the reciprocal Tchebycheff scalarizing function [33] and MOEA/D-PBI using the PBI scalarizing function [34].

The reciprocal Tchebycheff scalarizing function is defined as

$$\text{Minimize} \quad g^{\text{rTCH}}(\boldsymbol{x}|\boldsymbol{\lambda}) = \max_{i=1}^{m} |f_i(\boldsymbol{x}) - z_i|/\lambda_i. \tag{5}$$

The reciprocal Tchebycheff criterion complies with dominance, and MOEA/D-rTCH acquires non-dominated solutions approximating the Pareto front.

The PBI scalarizing function is defined as

$$\text{Minimize} \quad g^{\text{PBI}}(\boldsymbol{x}|\boldsymbol{\lambda}) = d_1(\boldsymbol{x}) + \theta d_2(\boldsymbol{x}), \tag{6}$$

where

$$d_1(\boldsymbol{x}) = \|(\boldsymbol{f}(\boldsymbol{x}) - \boldsymbol{z})^T \boldsymbol{\lambda}\|/\|\boldsymbol{\lambda}\|, \tag{7}$$

$$d_2(\boldsymbol{x}) = \|\boldsymbol{f}(\boldsymbol{x}) - (\boldsymbol{z} - d_1(\boldsymbol{x})\boldsymbol{\lambda}/\|\boldsymbol{\lambda}\|)\|\,, \tag{8}$$

$\boldsymbol{z}$ denotes the ideal point. d_2 is the perpendicular distance from objective vector $\boldsymbol{f}(\boldsymbol{x})$ to weight vector $\boldsymbol{\lambda}$. d_1 is the distance from the obtained ideal point $\boldsymbol{z}$ to the point that

perpendicularly projects $\boldsymbol{f}(\boldsymbol{x})$ on the weight vector $\boldsymbol{\lambda}$. For both d_1 and d_2, the shorter the value, the better it is. The balance between d_1 and d_2 is determined by parameter θ. The PBI criterion has a characteristic similar to directional dominance and acquires directionally non-dominated solutions approximating the directional Pareto front. The first equality condition in **Eq. (4)** is relaxed by parameter θ and encourages solution comparisons for each unit vector.

C. NSGA-III

NSGA-III [36] is an NSGA [37] algorithm series. To maintain a uniform distribution of the population in the objective space, NSGA-III uses perpendicular distances between solutions and reference lines, whereas NSGA-II [38] uses crowding distances, which are determined by the relative positions of the solutions in the objective space. Reference lines pass through the base and reference points, which are generated in the same manner as the weight vectors in MOEA/D.

In each generation, NSGA-III classifies the combined population of the parent and offspring populations into several fronts, solution sets, via non-dominated sorting. The parent population for the next generation is selected from the higher fronts with higher non-domination levels. Each parent candidate solution is paired with its closest reference line. A solution with a reference line having a small number of paired solutions and a solution with a shorter perpendicular distance is preferred as the parent population for the next generation.

Although NSGA-III uses a set of reference lines, non-dominated solutions are preferred and dominated solutions are not preferred as the parent population for the next population. NSGA-III acquires non-dominated solutions that approximate the Pareto front. Algorithms combining the dominance and the decomposition such as NSGA-III and MOEA/DD [39] tend to employ the dominance-based criterion with the first priority and the decomposition-based criterion with the second priority. Since the directionally non-dominated solutions involve dominated solutions that are discarded with the first priority, these algorithms cannot maintain the directionally non-dominated solutions in the population.

D. NSGA-II/SDR

NSGA-II/SDR [30] is based on NSGA-II and employs the strengthened dominance relation (SDR) instead of the conventional dominance relation used in conventional NSGA-II. For the two solutions, $\boldsymbol{x}$ and $\boldsymbol{y}$, $\boldsymbol{x}$ dominates $\boldsymbol{y}$ in SDR if and only if

$$\begin{cases} \sum_{i=1}^{m} f_i(\boldsymbol{x}) < \sum_{i=1}^{m} f_i(\boldsymbol{y}), & \theta_{\boldsymbol{xy}} \leq \overline{\theta}, \\ \sum_{i=1}^{m} f_i(\boldsymbol{x}) \cdot \frac{\theta_{\boldsymbol{xy}}}{\overline{\theta}} < \sum_{i=1}^{m} f_i(\boldsymbol{y}), & \theta_{\boldsymbol{xy}} > \overline{\theta}, \end{cases} \tag{9}$$

where $\theta_{\boldsymbol{xy}} = \cos^{-1}(\boldsymbol{f}(\boldsymbol{x}), \boldsymbol{f}(\boldsymbol{y}))$, and $\overline{\theta}$ is a user-defined angle. SDR uses a line passing through each objective vector and the base point. SDR strengthens the superiority judgment of solutions inside the angle $\overline{\theta}$ from the line. SDR weakens the superiority judgment of solutions outside the angle $\overline{\theta}$ from the line. SDR does not comply with dominance. A case arises in which two solutions are non-dominated in the SDR criterion, even if one dominates another in the conventional dominance when their angles differ greatly. SDR has a characteristic similar to directional dominance and acquires directionally, non-dominated solutions approximating the directional Pareto front. The first equality condition in **Eq. (4)** is relaxed by the user-defined angle $\overline{\theta}$ around each unit vector and encourages solution comparisons for each unit vector.

E. θ-DEA AND θ-DEA$^-$

θ-DEA [29] also uses a weight vector set. In each generation, θ-DEA performs two non-dominated sortings based on the conventional dominance and the θ-dominance sequentially.

Each solution is associated with its closest weight vector. Consequently, each weight vector creates a cluster of solutions. For the two solutions, $\boldsymbol{x}$ and $\boldsymbol{y}$, $\boldsymbol{x}$ θ-dominates $\boldsymbol{y}$ if and only if $\boldsymbol{x}$ and $\boldsymbol{y}$ are in the same cluster of a weight vector $\boldsymbol{\lambda}$ and $g^{\mathrm{PBI}}(\boldsymbol{x}|\boldsymbol{\lambda}) < g^{\mathrm{PBI}}(\boldsymbol{y}|\boldsymbol{\lambda})$. The two solutions in the different clusters are not θ-dominated. Two solutions in the same cluster are compared based on their PBI scalarizing function values.

The conventional θ-DEA discards directionally non-dominated solutions by non-dominated sorting based on conventional dominance and acquires non-dominated solutions that approximate the Pareto front. To obtain directionally non-dominated solutions, in this work, we employ a variant named θ-DEA$^-$, which disabled non-dominated sorting based on the conventional dominance.

F. RVEA AND RVEA*

The RVEA [35] also uses weight vectors and decomposes the objective space with them. RVEA performs a population partition in which each solution is associated with a weight vector with the minimum angle. In each parted population, RVEA selects the solution with the minimum APD (angle-penalized distance). APD is similar to PBI described as **Eq. (6)**. APD uses the norm of the objective vector $\boldsymbol{f}$ instead of d_1 and a relative angle between $\boldsymbol{f}$ and weight vector $\boldsymbol{\lambda}$ in the parted population instead of d_2. Consequently, APD also has a characteristic similar to the directional dominance. The first equality condition in **Eq. (4)** is relaxed by the angle-based penalty to the target weight vector and encourages solution comparisons for the weight vector.

RVEA does not involve non-dominated sorting and acquires directionally non-dominated solutions. The same study also proposed RVEA*, which arranges weight vectors to adopt irregular Pareto front shapes. RVEA* avoids having weight vectors for the non-existent area of the Pareto front in the objective space and acquires non-dominated solutions to approximate the Pareto front.

VII. EXPERIMENTAL SETUP

A. PROBLEMS

We used the DTLZ7 [25], UF9 [40], DTLZ1S1, and DTLZ1S2 problems. The number of objectives was set to

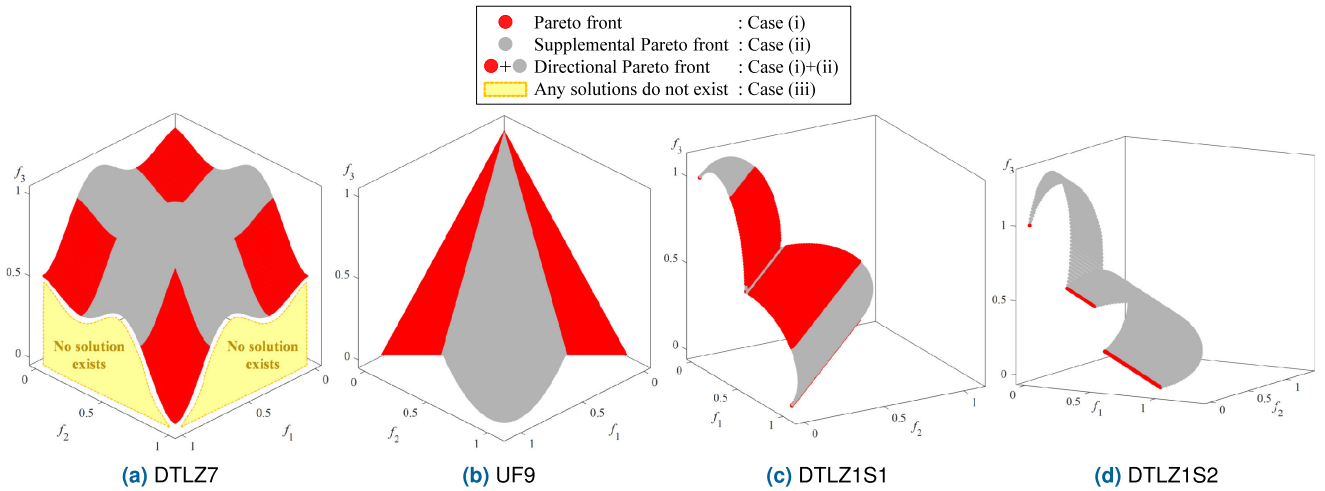

FIGURE 6. The Pareto front $\mathcal{F}^*$, the supplemental Pareto front $\mathcal{F}^-$, and the directional Pareto front $\mathcal{F}^+$.

$m = 3$, and the dimension of the variable space was set to $d = m - 1$. In addition, we normalized the range of the objective space to hold the Pareto front in $[0, 1]^{m=3}$. **Fig. 6** shows the objective spaces of their problems. As mentioned in Section V-B, each unit vector $\boldsymbol{e}$ in the objective space is classified into one of the cases (i), (ii), and (iii). In **Fig. 6**, unit vectors of the case (i) pass through the Pareto front $\mathcal{F}^*$ with red, unit vectors of the case (ii) pass through the supplemental Pareto front $\mathcal{F}^-$ with gray, and unit vectors of the case (iii) pass through the yellow area without any solutions. Note that the yellow areas are handwritten in **Fig. 6**. The two cases (ii) and (iii) are the non-existent area of the Pareto front. **Fig. 6 (b)** of UF9, **Fig. 6 (c)** of DTLZ1S1, and **Fig. 6 (d)** of DTLZ1S2 show the non-existent area of case (ii) only. **Fig. 6 (a)** of DTLZ7 shows the non-existent areas of both cases (ii) and (iii).

B. ALGORITHMS

We used MOEA/D-rTCH, MOEA/D-PBI, NSGA-III, NSGA-II/SDR, θ-DEA, θ-DEA$^-$, RVEA, and RVEA* algorithms. We expected that MOEA/D-rTCH, NSGA-III, θ-DEA, and RVEA* would obtain non-dominated solutions approximating the Pareto front. In addition, we expected that MOEA/D-PBI, NSGA-II/SDR, θ-DEA$^-$, and RVEA would obtain directionally non-dominated solutions approximating the directional Pareto front. Since the general aim of multi-objective optimization is the Pareto front approximation, note that any fair comparison of these algorithms for the directional Pareto front approximation cannot be conducted essentially. Note that experiments in this work aim to show the possible options to obtain directionally non-dominated solutions from the conventional candidate algorithms.

As common settings, we used simulated binary crossover (crossover ratio 1.0 and distribution index $\eta_c = 20$) and polynomial mutation (mutation ratio $1/d$ and distribution index $\eta_m = 20$). The population size is set to $N = 120$ and the total number of generations is set to $G = 3,000$. In MOEA/D, the neighborhood size was set to $T = 12$. For the PBI scalarizing function, $\theta = 10$ was employed. We utilized the implementation of PlatEMO [41]. Each algorithm was executed 31 times for each problem.

C. METRICS

For the approximation quality assessment of Pareto front $\mathcal{F}^*$, we used the conventional *IGD* [42]. *IGD* needs a reference objective vector set $\mathcal{R}$ that is a subset of the Pareto front $\mathcal{F}^*$, i.e. $\mathcal{R} \subseteq \mathcal{F}^*$. *IGD* is the average distance from every reference objective vector in $\mathcal{R}$ to its closest objective vector among the obtained solution set. For the approximation quality assessment of the directional Pareto front $\mathcal{F}^+$, in this work, we introduce *IGD*$'$ as an extension of the conventional *IGD*. *IGD*$'$ needs a reference objective vector set $\mathcal{R}'$ that is a subset of the directional Pareto front $\mathcal{F}^+$, i.e. $\mathcal{R}' \subseteq \mathcal{F}^+$. *IGD*$'$ is the average distance from every reference objective vector in $\mathcal{R}'$ to its closest objective vector among the obtained solution set. For both *IGD* and *IGD*$'$, the smaller the values, the better. Only the difference between the conventional *IGD* and *IGD*$'$ in this work is the reference sets $\mathcal{R}$ and $\mathcal{R}'$.

We describe how to generate the reference objective vector set $\mathcal{R}'$ for *IGD*$'$. For each of the DTLZ7 and UF9 problems, we first set a 100×100 grid on $f_1 - f_2$ space, then generated 10,000 points on the two-dimensional space, and calculated the third objective value based on f_1 and f_2 values for each point in the $f_1 - f_2$ space. We employed the generated 10,000 points in the $m = 3$-dimensional space as the reference set $\mathcal{R}'$. For the DTLZ1S1 and DTLZ1S2 problems, we generated 10,011 points uniformly distributed on the $m = 3$-dimensional hyperplane by using the simplex lattice [43], transformed them according to objective functions, and employed the transformed points as the reference set $\mathcal{R}'$. Note that the reference vector set $\mathcal{R}'$ contains the dominated points.

For the conventional *IGD*, we employed non-dominated points $\mathcal{R}$ extracted from $\mathcal{R}'$ generated by the above method

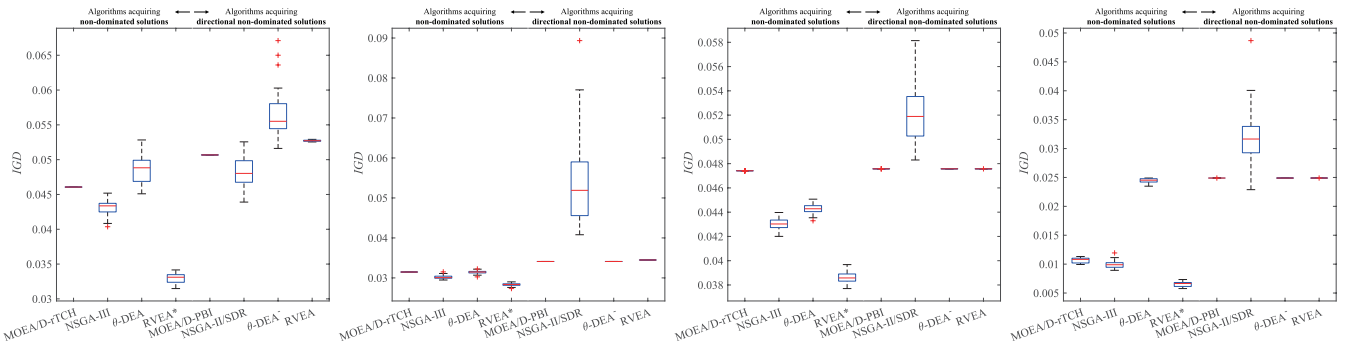

(a) DTLZ7 (b) UF9 (c) DTLZ1S1 (d) DTLZ1S2

FIGURE 7. *IGD* to assess the approximation quality of the Pareto front $\mathcal{F}^*$.

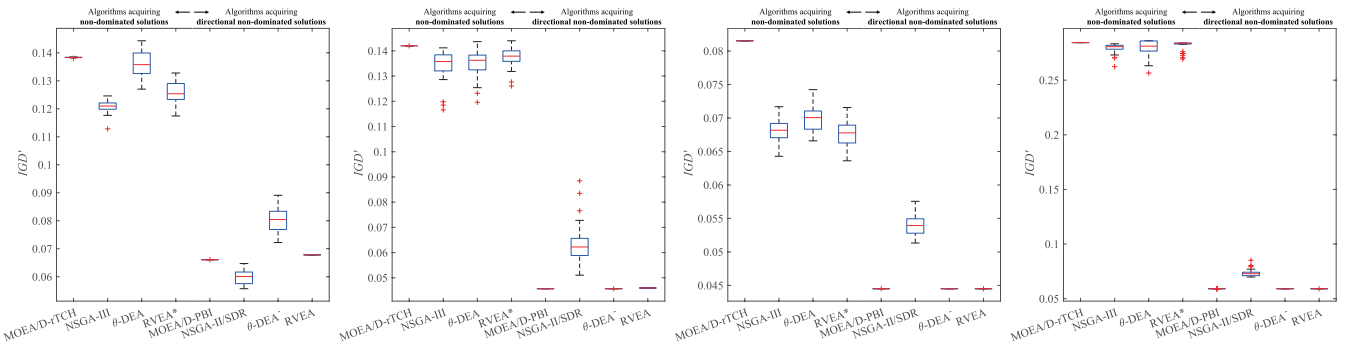

(a) DTLZ7 (b) UF9 (c) DTLZ1S1 (d) DTLZ1S2

FIGURE 8. *IGD*′ to assess the approximation quality of the directional Pareto front $\mathcal{F}^+$.

for each problem, i.e. $\mathcal{R} \subset \mathcal{R}'$. The sizes of the reference set $|\mathcal{R}|$ were 3,249, 5,050, 4,991, and 213 for DTLZ7, UF9, DTLZ1S1, and DTLZ1S2 problems, respectively.

VIII. EXPERIMENTAL RESULTS AND DISCUSSION

A. APPROXIMATION PERFORMANCE

Figs. 7 and 8 respectively show *IGD* and *IGD*′ values of 31 runs. In each figure, the four left box plots are the results of the four algorithms to acquire the non-dominated solutions. The four right box plots are the results of the four algorithms to acquire the directionally non-dominated solutions.

From the *IGD* viewpoint, to assess the Pareto front approximation quality in **Fig. 7**, we see that RVEA* is the best among all the problems. NSGA-II/SDR was the worst of the problems, except for DTLZ7. In UF9, all four algorithms acquiring non-dominated solutions showed a shorter *IGD* than all four algorithms acquiring directionally non-dominated solutions. However, this result was not necessarily related to other problems. In other words, there are several cases where algorithms acquiring directionally non-dominated solutions are comparable with algorithms acquiring non-dominated solutions from the *IGD* viewpoint. Because the Pareto front is a subset of the directional Pareto front, the search for the directional Pareto front contributes to acquiring non-dominated solutions approximating the Pareto front as well.

From the *IGD*′ viewpoint, to assess the directional Pareto front approximation quality in **Fig. 8**, we see that the remaining four algorithms acquiring the non-dominated solutions are worse than the right four algorithms acquiring the directionally non-dominated solutions in all problems.

Thus, MOEA/D-PBI, NSGA-II/SDR, θ-DEA$^-$, and RVEA acquiring directionally non-dominated solutions also work to approximate the Pareto front because the Pareto front is a subset of the targeting directional Pareto front. However, MOEA/D-rTCH, NSGA-III, θ-DEA, and RVEA* acquiring non-dominated solutions do not approximate the directional Pareto front because the directional Pareto front is a superset of the targeting Pareto front. For the Pareto front approximation, the algorithms acquiring directionally non-dominated solutions are not better than the algorithms acquiring non-dominated solutions. However, directionally non-dominated solutions are a value-added output that provides solutions representing not only the Pareto front but also the objective value change in the area where the Pareto front does not exist.

B. OBTAINED NON-DOMINATED AND DIRECTIONALLY NON-DOMINATED SOLUTIONS

Figs. 9–16 show solution sets obtained by the eight different algorithms on four different problems. **Fig. 6** will be the reference to discuss the obtained solution distributions. In **Fig. 6**,

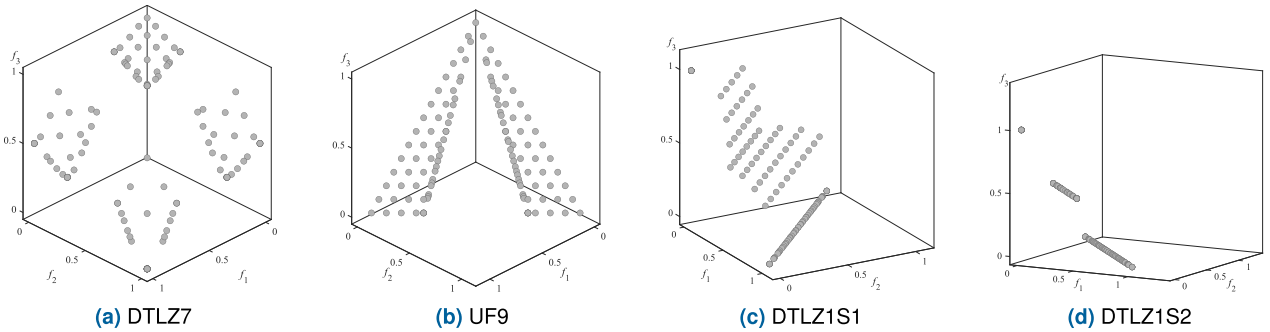

FIGURE 9. Solutions obtained by MOEA/D-rTCH.

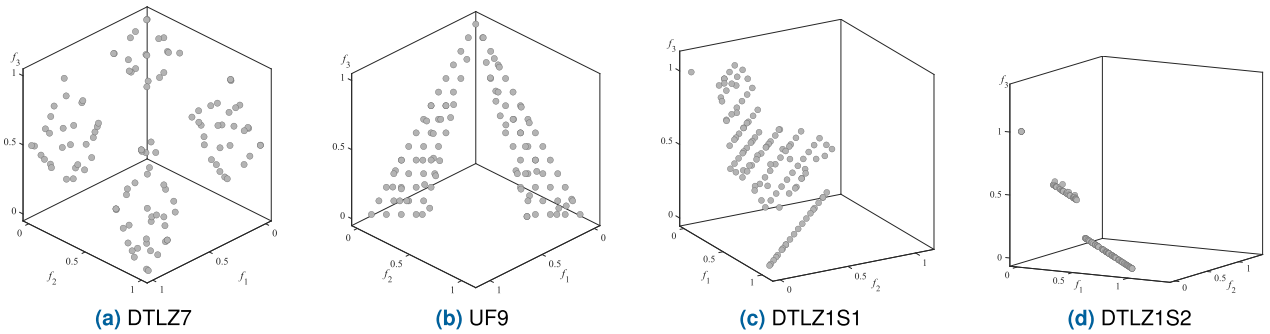

FIGURE 10. Solutions obtained by NSGA-III.

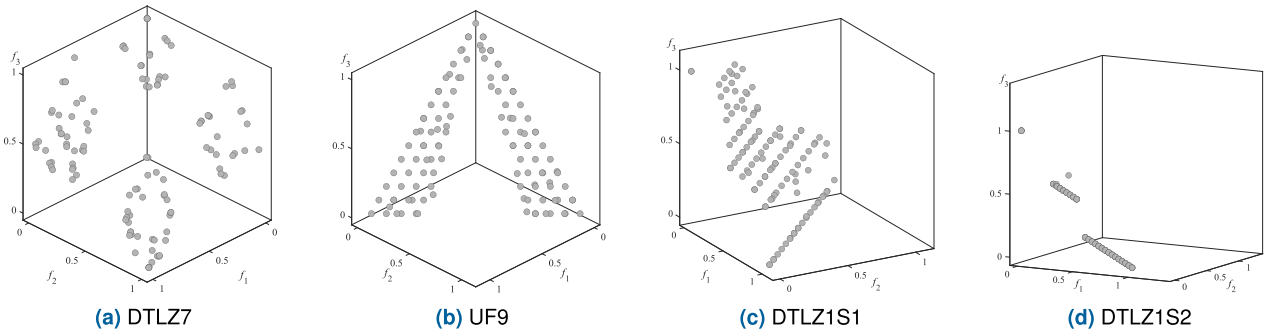

FIGURE 11. Solutions obtained by θ-DEA.

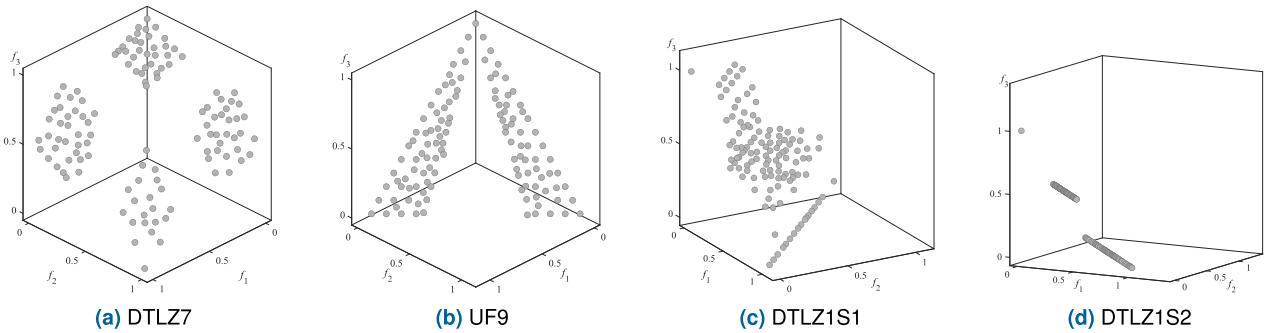

FIGURE 12. Solutions obtained by RVEA*.

the Pareto front is red, supplemental Pareto front is gray, and directional Pareto front is red and gray. In **Figs. 9–16**, obtained solutions are gray.

Figs. 9–12 are results obtained by MOEA/D-rTCH, NSGA-III, θ-DEA, and RVEA*, which acquire the non-dominated solutions to approximate the Pareto front. These

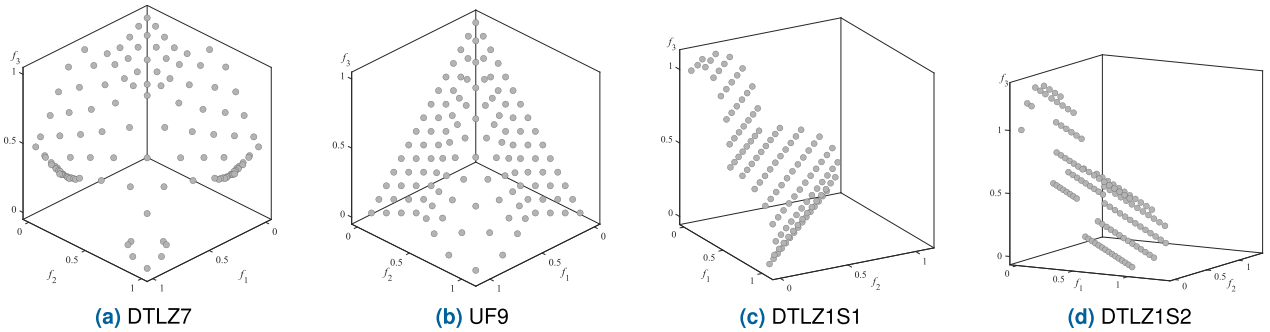

(a) DTLZ7 (b) UF9 (c) DTLZ1S1 (d) DTLZ1S2

FIGURE 13. Solutions obtained by MOEA/D-PBI.

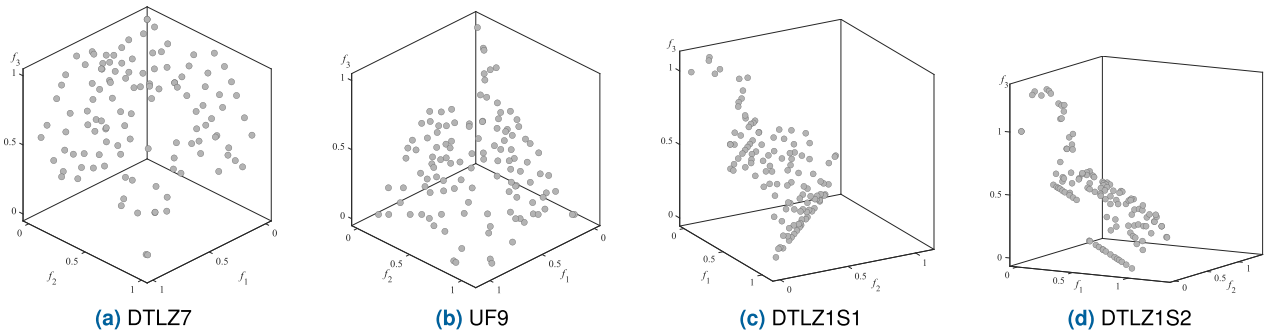

(a) DTLZ7 (b) UF9 (c) DTLZ1S1 (d) DTLZ1S2

FIGURE 14. Solutions obtained by NSGA-II/SDR.

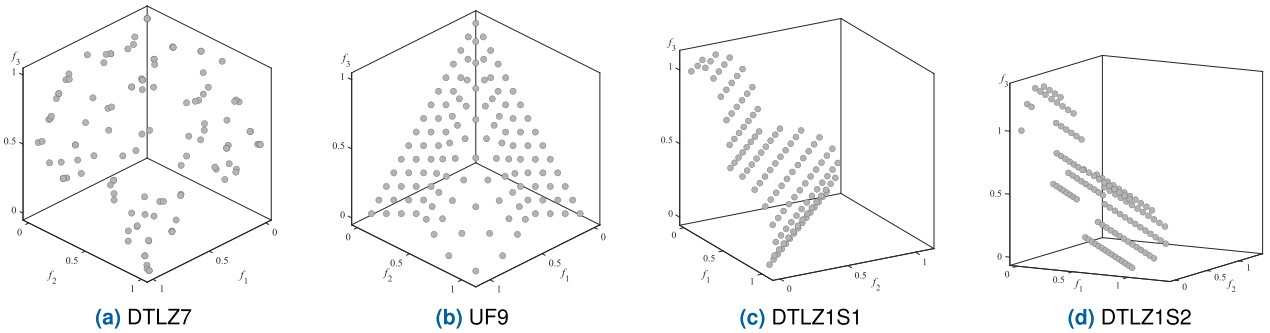

(a) DTLZ7 (b) UF9 (c) DTLZ1S1 (d) DTLZ1S2

FIGURE 15. Solutions obtained by θ-DEA^{-}.

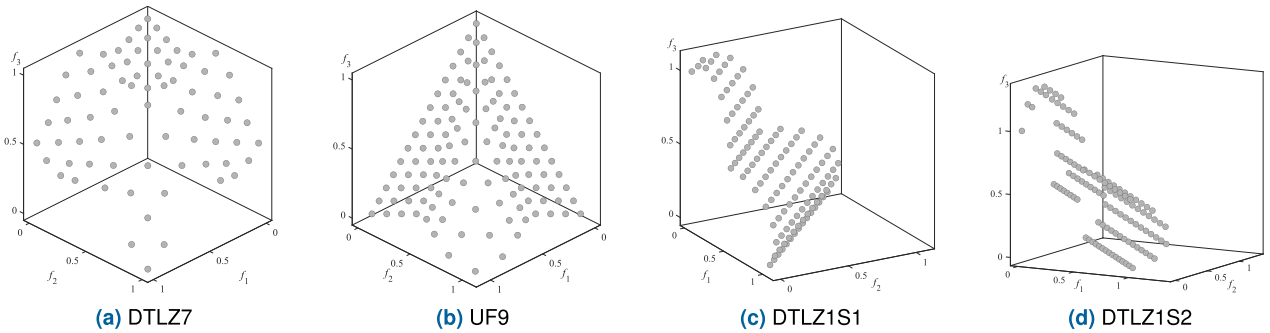

(a) DTLZ7 (b) UF9 (c) DTLZ1S1 (d) DTLZ1S2

FIGURE 16. Solutions obtained by RVEA.

results indicate that the obtained solutions were gapped in the objective space. Nothing explains the gap in each objective space, because the obtained solutions only approximate and represent the Pareto front. In particular, in DTLZ1S2, these four algorithms obtained solutions only in limited areas of the objective space. The decision maker might have doubts

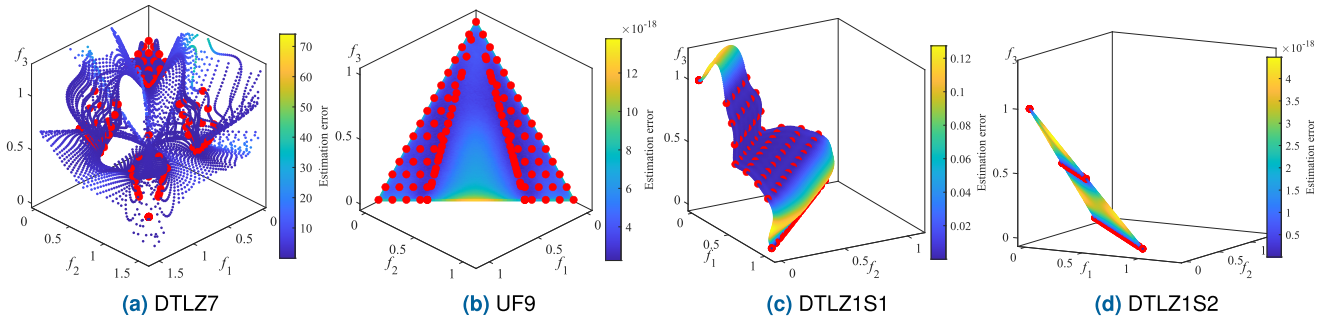

FIGURE 17. Response surface using solutions obtained by MOEA/D-rTCH.

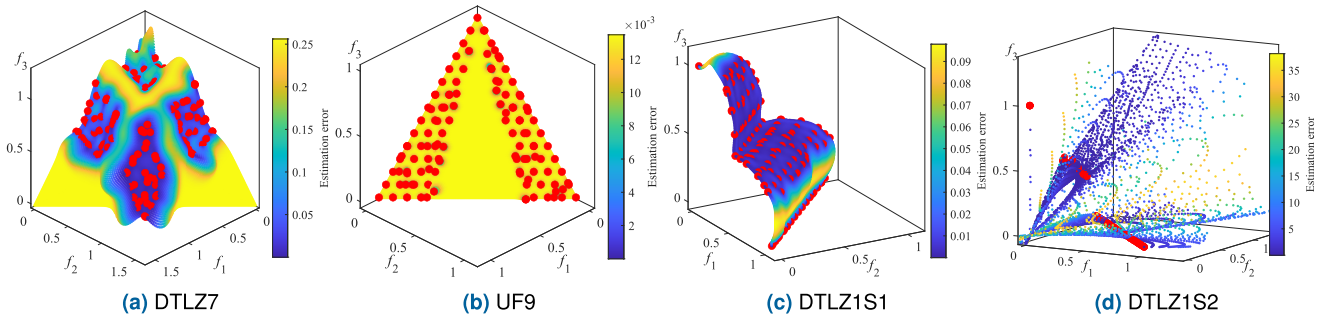

FIGURE 18. Response surface using solutions obtained by NSGA-III.

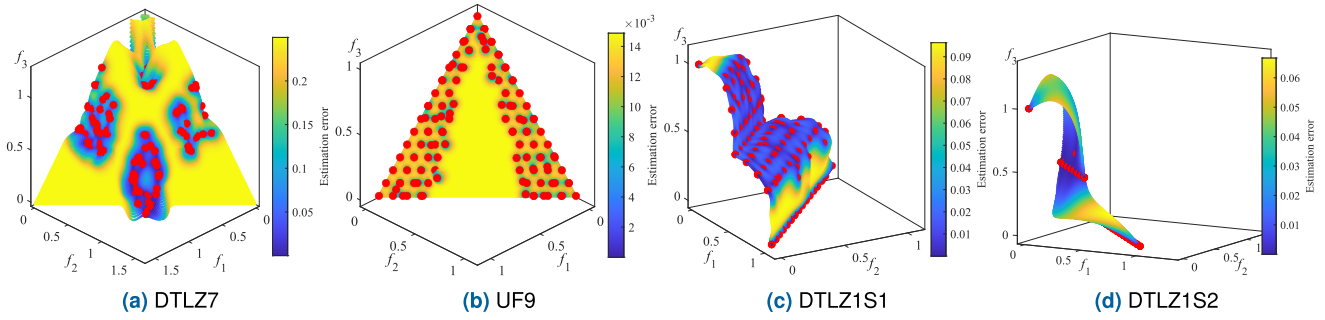

FIGURE 19. Response surface using solutions obtained by θ-DEA.

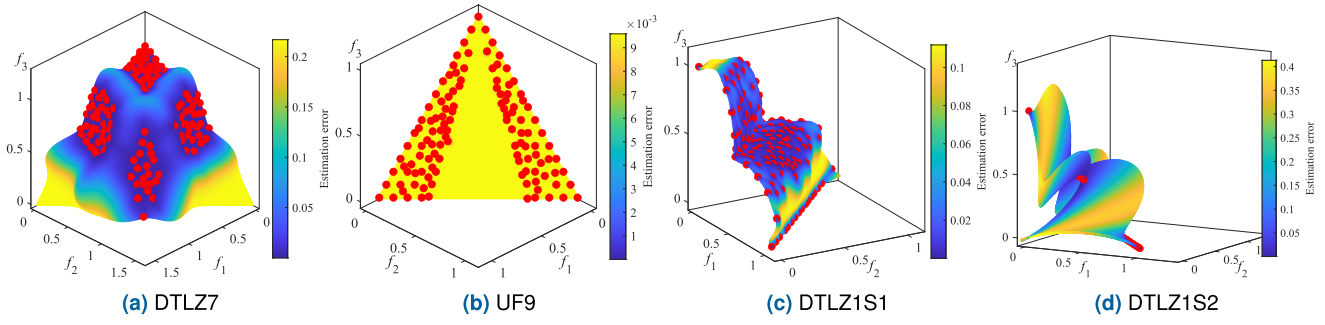

FIGURE 20. Response surface using solutions obtained by RVEA*.

about the optimization result, such as whether there are other optimal trade-offs among the objectives.

Figs. 13–16 are results obtained by MOEA/D-PBI, NSGA-II/SDR, θ-DEA$^-$, and RVEA, which acquire the directionally non-dominated solutions to approximate the directional Pareto front. We can see that these algorithms obtain solutions that approximate the directional Pareto front involving the Pareto front and the supplemental Pareto front.

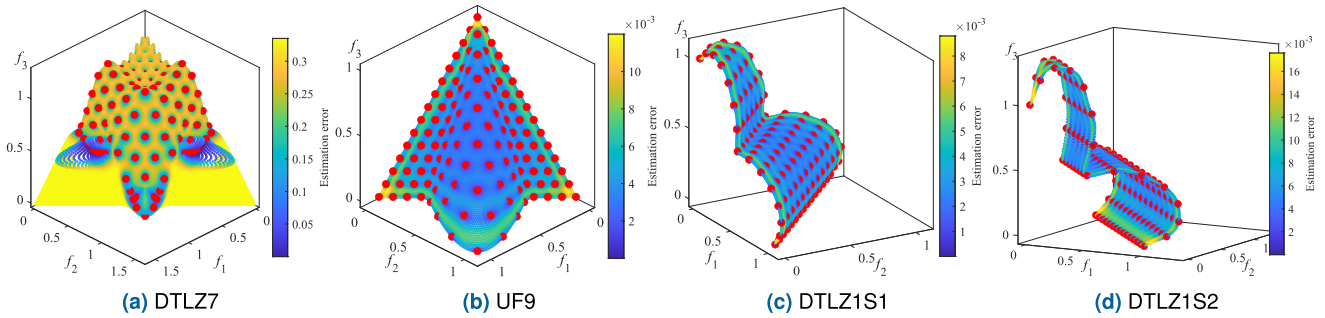

FIGURE 21. Response surface using solutions obtained by MOEA/D-PBI.

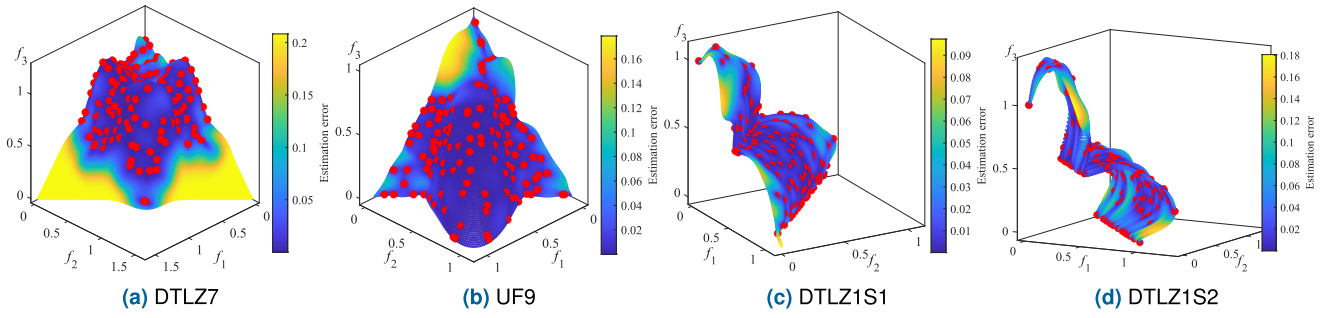

FIGURE 22. Response surface using solutions obtained by NSGA-II/SDR.

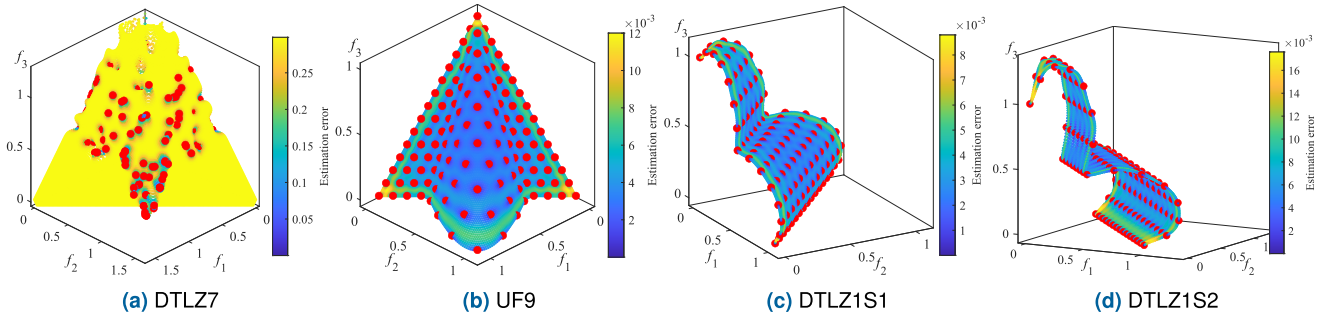

FIGURE 23. Response surface using solutions obtained by θ-DEA^{-}.

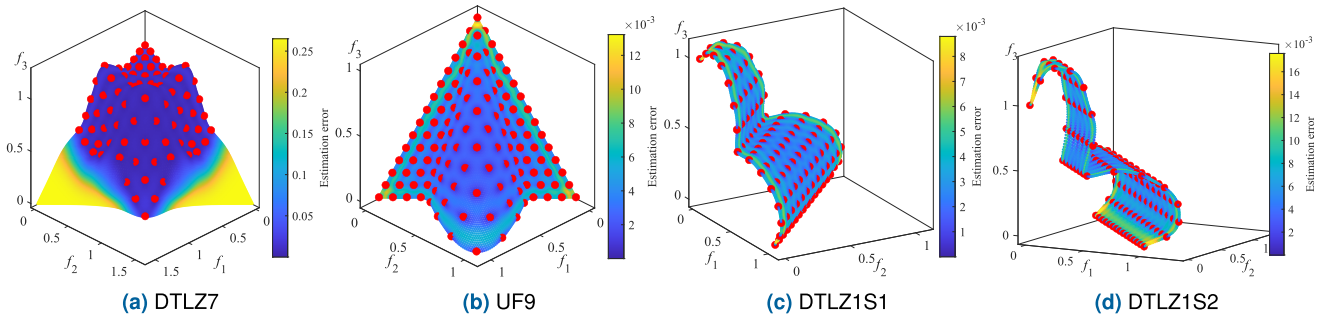

FIGURE 24. Response surface using solutions obtained by RVEA.

These algorithms explain the objective value change, even in the non-existence area of the Pareto front in the objective space. However, because these algorithms require solutions to represent the supplemental Pareto front, they cannot avoid deteriorating the resolution required to approximate the Pareto front. In the case of DTLZ7, there are areas where no solution exists, as shown in **Fig. 6 (a)** with yellow. From **Figs. 9–16 (a)**, we see that even algorithms acquiring

directionally non-dominated solutions do not obtain any solutions in the yellow areas of **Fig. 6 (a)**.

C. ESTIMATED PARETO FRONT AND ESTIMATED DIRECTIONAL PARETO FRONT

Figs. 17–24 show unit hyperplane-based response surfaces constructed by the obtained solutions. Red points indicate the obtained solutions. A huge set of points with a color gradation from blue to yellow indicates the estimated value. The color indicates the confidence level of the estimated value. **Fig. 6** will be the reference to discuss the results of the obtained response surfaces.

We discuss **Figs. 17–20** obtained by MOEA/D-rTCH, NSGA-III, θ-DEA, and RVEA*, which acquire the non-dominated solutions. First, we focused on (a) DTLZ7. We can see that the solution distribution is biased on the Pareto front area, which deteriorates the accuracy of the Pareto front estimation. It can be seen especially in the results with MOEA/D-rTCH. In addition, we see that NSGA-III and θ-DEA have few solutions around the f_3 axis, which causes low estimation accuracy of the Pareto front part. Next, we examined the supplemental Pareto front areas. Estimating the supplemental Pareto front using only non-dominated solutions is a difficult task. RVEA* obtained solutions with a low distribution bias and showed a relatively high estimation accuracy for the supplemental Pareto front. In (b) UF9, all four algorithms face difficulty in estimating the supplemental Pareto front between the two groups of obtained non-dominated solutions. In addition, in (c) DTLZ1S1, we observed a low estimation accuracy of the supplemental Pareto front. In the extreme case (d) DTLZ1S2, we saw a high distribution bias of the obtained solution and difficulty in estimating the supplemental Pareto front using only non-dominated solutions.

We discuss **Figs. 21–24** obtained by MOEA/D-PBI, NSGA-II/SDR, θ-DEA$^-$, and RVEA, which acquire the directionally non-dominated solutions. We see a high estimation accuracy of the directional Pareto front involving the Pareto front and the supplemental Pareto front. The population sizes shown in **Figs. 17–20** and **Figs. 21–24** are the same. The solutions in **Figs. 17–20** only represent the Pareto front which exists in the limited area of the objective space. By contrast, the solutions in **Figs. 21–24** need to represent not only the Pareto front but also the supplemental Pareto front. Consequently, in **Figs. 21–24**, algorithms have to decrease the solution distribution density. This influence can be seen in the results of NSGA-II/SDR on all problems and θ-DEA$^-$ on DTLZ7. The difficulty of local convergence in the objective space also affects the local estimation accuracy of the directional Pareto front. To improve the estimation accuracy of the directional Pareto front, an increase in the population size and number of generations is a promising option. In the case of DTLZ7, there are areas where no solution exists, as shown in **Fig. 6 (a)** with yellow. Each of **Figs. 17–24 (a)** represents a response surface, even in the yellow areas of **Fig. 6 (a)**. For this case, it is useful to observe the directionally non-dominated solution set and its response surface simultaneously. The parts of the response surface without directionally non-dominated solutions could suggest the non-existent area of the Pareto front and any solutions, which is the case (iii) described in Section V-B.

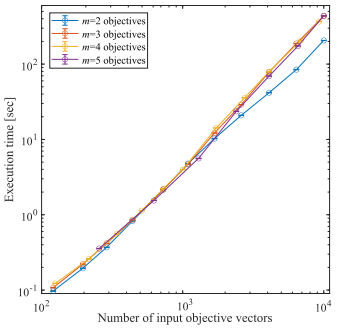

FIGURE 25. Execution times to obtain the unit hyperplane-based response surfaces when the numbers of input objective vectors and objectives *m* changes on DTLZ7.

Solutions that contribute to the estimation of the supplemental Pareto front are dominated solutions that are generally discarded in multi-objective optimization. However, these solutions can be utilized to represent the objective value trade-off of non-existent areas of non-dominated solutions. The directional Pareto front and the estimated front enhance the explanation of the objective space and encourage multi-objective decision making, especially in the case where the Pareto front exists in limited regions in the objective space.

D. COMPUTATIONAL TIME

We measured the execution time in obtaining the unit hyperplane-based response surface. We used a computer with AMD Ryzen Threadripper 3970X CPU, 32GB memory, Windows 10 operating system, and MATLAB as the implementation environment. We here picked DTLZ7 and prepared multiple input objective vector sets with different sizes.[1] **Fig. 25** shows the results. The size of the input objective vectors is varied by the horizontal axis. **Fig. 25** involves four lines with different numbers of objectives m. For each of the response surfaces respectively in $m = \{2, 3, 4, 5\}$ objectives, we estimate objective vectors on 10011, 10011, 9880, and 8855 uniformly distributed L^1 unit vectors generated by the simplex lattice method. The vertical axis is the execution time, and note that it is a logarithmic scale. The results show

[1] We generated input objective vector sets on the directional Pareto front by utilizing the problem definition of DTLZ7 in the same manner to generate the reference set R' for IGD' described in Section VII-C. For m objective DTLZ7, we first considered $m-1$ dimensional objective space $[0, 1]^{m-1}$ of $f_1, \ldots, f_{m-1}$. We set a grid in which each of $m-1$ objective dimensions is h equally spaced. We then obtained h^{m-1} evenly distributed grid points in the $m-1$ dimensional objective space. For each grid point including $f_1, \ldots, f_{m-1}$ objective values, we could calculate f_m based on the definition of DTLZ7. The above process obtained h^{m-1} input objective vectors. For multiple input objective vector sets with different sizes, we here used $h = \{121, 196, 289, 441, 729, 1089, 1681, 2601, 4096, 6400, 10000\}$ for $m = 2$, $h = \{11, 14, 17, 21, 27, 33, 41, 51, 64, 80, 100\}$ for $m = 3$, $h = \{5, 6, 7, 8, 9, 10, 12, 14, 16, 19, 21\}$ for $m = 4$, and $h = \{4, 5, 6, 7, 8, 9, 10\}$ for $m = 5$.

that the execution time is affected by the size of the input objective vectors rather than the number of objectives m.

For the Pareto front that may involve an infinite number of objective vectors, there is an essential difference between discretely representing the Pareto front with a set of points of objective vectors and near-continuously representing the Pareto front with the unit hyperplane-based response surface. In the optimization of computationally cheap objective functions, the time to evaluate each solution is short, and it is relatively easy to plot many points of objective vectors for the approximation quality improvement of the Pareto front. In the optimization of computationally expensive objective functions, the time to evaluate each solution is long, and it is relatively difficult to plot many points of objective vectors for the approximation quality improvement of the Pareto front. Since the unit hyperplane-based response surface represents objective value change among a limited number of objective vectors, there would be demand, especially for optimization problems with computationally expensive objective functions. The results in **Fig. 25** could be a guide to consider whether or not to employ the unit hyperplane-based response surface method by comparing its execution time and the time of repeatedly executing objective functions in each optimization problem.

IX. CONCLUSION

To encourage multi-objective decision making, especially in the case where the Pareto front exists in limited regions, we introduced the concepts of the directional Pareto front involving the supplemental Pareto front, which shows the objective value trade-off even in areas where the Pareto front does not exist. In addition, we employed the unit hyperplane-based response surface method to smoothly estimate the directional Pareto front using a limited number of objective vectors and the examined solutions. The experimental results showed that the non-dominated solutions obtained by general evolutionary multi-objective optimization are not sufficient to represent the objective value trade-off in areas where the Pareto front does not exist, even when the unit hyperplane-based response surface method is used. We showed that the directionally non-dominated solutions obtained by evolutionary algorithms employing solution comparison criteria relaxing the directional dominance provide not only non-dominated solutions approximating the Pareto front but also solutions representing the objective value trade-off in areas where the Pareto front does not exist. These algorithms sacrifice the approximation resolution of the Pareto front because they require solutions to approximate the objective value trade-off in the non-existence area of the Pareto front. In particular, when the Pareto front exists in limited regions, it provides an explanation of the objective space, which cannot be provided by non-dominated solutions. In addition, we showed that the unit hyperplane-based response surface method complements the directional Pareto front approximation, even though directionally non-dominated solutions are sparsely distributed.

In future work, we will deepen the design of evolutionary algorithms to acquire directionally non-dominated solutions approximating the directional Pareto front. A decomposition-based approach will be a promising baseline for this task. External archive of non-dominated solutions is often employed for the improvement of the Pareto front approximation. This idea could be extended to the directional Pareto front approximation by introducing a criterion to maintain directionally non-dominated solutions to the new external archive. Then, even if an algorithm searches for the Pareto front, directionally non-dominated solutions generated during the search can be stored in the new external archive. However, if the algorithm searches for the Pareto front, we need to recognize that a high approximation quality of the supplemental Pareto front would not be expected with this idea. As the approximation performance metrics, this work used the IGD' known reference points on the directional Pareto front. We designed a performance metric for unknown problems, which does not require any problem knowledge.

REFERENCES

[1] K. Deb, *Multi-Objective Optimization Using Evolutionary ALG*. Hoboken, NJ, USA: Wiley, 2001.

[2] C. A. C. Coello, G. B. Lamont, and D. A. Van Veldhuizen, *Evolutionary Algorithms for Solving Multi-Objective Problems*. Cham, Switzerland: Springer, 2007.

[3] V. Chankong and Y. Y. Haimes, *Multiobjective Decision Making: Theory and Methodology*. New York, NY, USA: Dover, 2008.

[4] Y. Hua, Q. Liu, K. Hao, and Y. Jin, "A survey of evolutionary algorithms for multi-objective optimization problems with irregular Pareto fronts," *IEEE/CAA J. Autom. Sinica*, vol. 8, no. 2, pp. 303–318, Feb. 2021.

[5] R. Cheng, M. Li, Y. Tian, X. Zhang, S. Yang, Y. Jin, and X. Yao, "A benchmark test suite for evolutionary many-objective optimization," *Complex Intell. Syst.*, vol. 3, no. 1, pp. 67–81, Mar. 2017.

[6] Y. Liu, H. Ishibuchi, N. Masuyama, and Y. Nojima, "Adapting reference vectors and scalarizing functions by growing neural gas to handle irregular Pareto fronts," *IEEE Trans. Evol. Comput.*, vol. 24, no. 3, pp. 439–453, May 2019.

[7] H. Ishibuchi, L. He, and K. Shang, "Regular Pareto front shape is not realistic," in *Proc. IEEE Congr. Evol. Comput.*, Jun. 2019, pp. 2034–2041.

[8] T. Takagi, K. Takadama, and H. Sato, "Pareto front estimation using unit hyperplane," in *Proc. Int. Conf. Evol. Multi-Criterion Optim.*, in Lecture Notes in Computer Science, vol. 12654. Cham, Switzerland: Springer, 2021, pp. 126–138.

[9] A. G. Hernández-Díaz, L. V. Santana-Quintero, C. A. C. Coello, and J. Molina, "Pareto-adaptive ε-dominance," *Evol. Comput.*, vol. 15, no. 4, pp. 493–517, 2007.

[10] S. Zapotecas Martínez, V. A. Sosa Hernández, H. Aguirre, K. Tanaka, and C. A. C. Coello, "Using a family of curves to approximate the Pareto front of a multi-objective optimization problem," in *Proc. Int. Conf. Parallel Problem Solving Nature*. Cham, Switzerland: Springer, 2014, pp. 682–691.

[11] A. Zhou, Q. Zhang, and Y. Jin, "Approximating the set of Pareto-optimal solutions in both the decision and objective spaces by an estimation of distribution algorithm," *IEEE Trans. Evol. Comput.*, vol. 13, no. 5, pp. 1167–1189, Oct. 2009.

[12] Y. Tian, X. Zhang, R. Cheng, C. He, and Y. Jin, "Guiding evolutionary multiobjective optimization with generic front modeling," *IEEE Trans. Cybern.*, vol. 50, no. 3, pp. 1106–1119, Mar. 2020.

[13] Y. Tian, L. Si, X. Zhang, K. C. Tan, and Y. Jin, "Local model-based Pareto front estimation for multiobjective optimization," *IEEE Trans. Syst., Man, Cybern., Syst.*, vol. 53, no. 1, pp. 623–634, Jan. 2023.

[14] M. Hartikainen, K. Miettinen, and M. M. Wiecek, "PAINT: Pareto front interpolation for nonlinear multiobjective optimization," *Comput. Optim. Appl.*, vol. 52, no. 3, pp. 845–867, Jul. 2012.

[15] K. S. Bhattacharjee, H. K. Singh, and T. Ray, "An approach to generate comprehensive piecewise linear interpolation of Pareto outcomes to aid decision making," *J. Global Optim.*, vol. 68, no. 1, pp. 71–93, May 2017.

[16] K. S. Bhattacharjee, H. K. Singh, and T. Ray, "Enhanced Pareto interpolation method to aid decision making for discontinuous Pareto optimal fronts," in *Proc. Australas. Joint Conf. Artif. Intell.* Cham, Switzerland: Springer, 2017, pp. 93–105.
[17] K. Kobayashi, N. Hamada, A. Sannai, A. Tanaka, K. Bannai, and M. Sugiyama, "Bézier simplex fitting: Describing Pareto fronts of simplicial problems with small samples in multi-objective optimization," in *Proc. AAAI Conf. Artif. Intell.*, 2019, vol. 33, no. 1, pp. 2304–2313.
[18] R. H. Myers, D. C. Montgomery, and C. M. Anderson-Cook, *Response Surface Methodology: Process and Product Optimization Using Designed Experiments*. Hoboken, NJ, USA: Wiley, 2016.
[19] I. J. Schoenberg, "Metric spaces and completely monotone functions," *Ann. Math.*, vol. 39, no. 4, pp. 811–841, Oct. 1938.
[20] J. Liu, *Radial Basis Function (RBF) Neural Network Control for Mechanical Systems: Design, Analysis and MATLAB Simulation*. Cham, Switzerland: Springer, 2013.
[21] I. Giagkiozis and P. J. Fleming, "Increasing the density of available Pareto optimal solutions," Autom. Control Syst. Eng., Univ. Sheffield, Sheffield, U.K., Tech. Rep., 1028, 2012.
[22] I. Giagkiozis and P. J. Fleming, "Pareto front estimation for decision making," *Evol. Comput.*, vol. 22, no. 4, pp. 651–678, Dec. 2014.
[23] M. L. Stein, *Interpolation of Spatial Data: Some Theory for Kriging*. Cham, Switzerland: Springer, 2012.
[24] J. Sacks, W. J. Welch, T. J. Mitchell, and H. P. Wynn, "Design and analysis of computer experiments," *Stat. Sci.*, vol. 4, no. 4, pp. 409–423, 1989.
[25] K. Deb, L. Thiele, M. Laumanns, and E. Zitzler, "Scalable multi-objective optimization test problems," in *Proc. IEEE Congr. Evol. Comput.*, May 2002, pp. 825–830.
[26] M. Laumanns, L. Thiele, K. Deb, and E. Zitzler, "Combining convergence and diversity in evolutionary multiobjective optimization," *Evol. Comput.*, vol. 10, no. 3, pp. 263–282, 2002.
[27] H. Sato, H. E. Aguirre, and K. Tanaka, "Controlling dominance area of solutions and its impact on the performance of MOEAs," in *Proc. Int. Conf. Evol. Multi-Criterion Optim.*, in Lecture Notes in Computer Science, vol. 4403. Cham, Switzerland: Springer, 2007, pp. 5–20.
[28] L. S. Batista, F. Campelo, F. G. Guimaraes, and J. A. Ramírez, "Pareto cone ε-dominance: Improving convergence and diversity in multiobjective evolutionary algorithms," in *Proc. Int. Conf. Evol. Multi-Criterion Optim.*, in Lecture Notes in Computer Science, vol. 6576. Cham, Switzerland: Springer, 2011, pp. 76–90.
[29] Y. Yuan, H. Xu, B. Wang, and X. Yao, "A new dominance relation-based evolutionary algorithm for many-objective optimization," *IEEE Trans. Evol. Comput.*, vol. 20, no. 1, pp. 16–37, Feb. 2016.
[30] Y. Tian, R. Cheng, X. Zhang, Y. Su, and Y. Jin, "A strengthened dominance relation considering convergence and diversity for evolutionary many-objective optimization," *IEEE Trans. Evol. Comput.*, vol. 23, no. 2, pp. 331–345, Apr. 2019.
[31] J. Shen, P. Wang, and X. Wang, "A controlled strengthened dominance relation for evolutionary many-objective optimization," *IEEE Trans. Cybern.*, vol. 52, no. 5, pp. 3645–3657, May 2022.
[32] V. J. Bowman, "On the relationship of the Tchebycheff norm and the efficient frontier of multiple-criteria objectives," in *Multiple Criteria Decision Making*. Berlin, Germany: Springer, 1976, pp. 76–86.
[33] K. Li, Q. Zhang, S. Kwong, M. Li, and R. Wang, "Stable matching-based selection in evolutionary multiobjective optimization," *IEEE Trans. Evol. Comput.*, vol. 18, no. 6, pp. 909–923, Dec. 2013.
[34] Q. Zhang and H. Li, "MOEA/D: A multiobjective evolutionary algorithm based on decomposition," *IEEE Trans. Evol. Comput.*, vol. 11, no. 6, pp. 712–731, Dec. 2007.
[35] R. Cheng, Y. Jin, M. Olhofer, and B. Sendhoff, "A reference vector guided evolutionary algorithm for many-objective optimization," *IEEE Trans. Evol. Comput.*, vol. 20, no. 5, pp. 773–791, Oct. 2016.
[36] K. Deb and H. Jain, "An evolutionary many-objective optimization algorithm using reference-point-based nondominated sorting approach, Part I: Solving problems with box constraints," *IEEE Trans. Evol. Comput.*, vol. 18, no. 4, pp. 577–601, Aug. 2013.
[37] N. Srinivas and K. Deb, "Muiltiobjective optimization using nondominated sorting in genetic algorithms," *Evol. Comput.*, vol. 2, no. 3, pp. 221–248, 1994.
[38] K. Deb, A. Pratap, S. Agarwal, and T. Meyarivan, "A fast and elitist multiobjective genetic algorithm: NSGA-II," *IEEE Trans. Evol. Comput.*, vol. 6, no. 2, pp. 182–197, Aug. 2002.
[39] K. Li, K. Deb, Q. Zhang, and S. Kwong, "An evolutionary many-objective optimization algorithm based on dominance and decomposition," *IEEE Trans. Evol. Comput.*, vol. 19, no. 5, pp. 694–716, Oct. 2015.
[40] Q. Zhang, A. Zhou, S. Zhao, P. N. Suganthan, W. Liu, and S. Tiwari, "Multiobjective optimization test instances for the CEC 2009 special session and competition," Univ. Essex Nanyang Technol. Univ., Singapore, Tech. Rep., CES-887, 2008.
[41] Y. Tian, R. Cheng, X. Zhang, and Y. Jin, "Platemo: A MATLAB platform for evolutionary multi-objective optimization," *IEEE Comput. Intell. Mag.*, vol. 12, no. 4, pp. 73–87, Nov. 2017.
[42] S. Jiang, Y.-S. Ong, J. Zhang, and L. Feng, "Consistencies and contradictions of performance metrics in multiobjective optimization," *IEEE Trans. Cybern.*, vol. 44, no. 12, pp. 2391–2404, Dec. 2014.
[43] I. Das and J. E. Dennis, "Normal-boundary intersection: A new method for generating the Pareto surface in nonlinear multicriteria optimization problems," *SIAM J. Optim.*, vol. 8, no. 3, pp. 631–657, Jul. 1998.

TOMOAKI TAKAGI (Graduate Student Member, IEEE) received the B.E. and M.E. degrees from The University of Electro-Communications, Japan, in 2018 and 2020, respectively, where he is currently pursuing the Ph.D. degree. His research interests include evolutionary multi- and many-objective optimization and its applications. He is also a Student Member of the Japanese Society for Evolutionary Computation.

KEIKI TAKADAMA (Member, IEEE) received the M.E. degree from Kyoto University, Japan, in 1995, and the Doctor of Engineering degree from The University of Tokyo, Japan, in 1998. He worked with the Tokyo Institute of Technology as a Lecturer, from 2002 to 2006. He moved to The University of Electro-Communications as an Associate Professor, in 2006. He has been a Professor, since 2011. His research interests include multiagent systems, distributed artificial intelligence, autonomous systems, reinforcement learning, learning classifier systems, and emergent computation. He is also a member of major AI- and informatics-related academic societies in Japan.

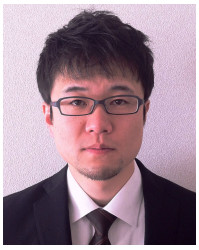

HIROYUKI SATO (Member, IEEE) received the B.E., M.E., and Ph.D. degrees from Shinshu University, Japan, in 2003, 2005, and 2009, respectively. He has been working with The University of Electro-Communications, since 2009. He is currently an Associate Professor. His research interests include evolutionary multi- and many-objective optimization and its applications. He is also a member of the Japanese Society for Evolutionary Computation. He received best paper awards in GECCO 2011, 2014, and 2022, and the Transaction of the Japanese Society for Evolutionary Computation, in 2012, 2015, 2020, and 2022.